The Journal of Navigation (2022), **75**:5 1190–1205
doi:10.1017/S0373463322000431

CAMBRIDGE UNIVERSITY PRESS

RESEARCH ARTICLE

Sea current relative navigation using interacting multiple model filter with adaptive fading technique

Jaehyuck Cha,[1] Jeong Ho Hwang,[1] and Chan Gook Park[1,2]*

[1] Mechanical and Aerospace Engineering/Automation and System Research Institute, Seoul National University, Seoul, South Korea
[2] Institute of Advanced Aerospace Technology, Seoul National University, Seoul, South Korea.
*Corresponding author. E-mail: chanpark@snu.ac.kr

Received: 1 November 2021; **Accepted:** 19 July 2022; **First published online:** 22 August 2022

Keywords: underwater navigation; Doppler velocity log; electro-magnetic log; current; adaptive Kalman filter

Abstract

In this paper, we propose a sea current relative navigation method using an interacting multiple model (IMM) filter with adaptive fading technique that can compensate an inaccurate sea current dynamics model. Due to the marine environment, the underwater vehicles largely depend on inertial navigation. Unfortunately, since its performance deteriorates with time, it is usually aided by another sensor. An electromagnetic-log (EM-log) and a Doppler velocity log (DVL), which are mainly used in marine navigation, provide relative velocity measurements to the sea currents, and hence require an accurate sea current dynamics model to fully utilise them. However, it is difficult to reflect the actual sea current changes with just a single fixed model, resulting in degraded overall navigation performance. Therefore, this paper proposes an IMM filter that can use multiple sea current dynamics models and has sub-filters designed with adaptive fading extended Kalman filter (AFEKF) to compensate for the mismodelling of sea current dynamics. The method is verified by simulation and shows a performance improvement comparable to the optimal filter.

1. Introduction

Recently, underwater vehicles are operating in the ocean to perform a variety of missions. For such operations, a proper navigation system that accurately estimates the position and the attitude of the vehicles is required. The global navigation satellite system (GNSS) is a widely used navigation system (Groves, 2013). However, since the satellite signal quickly attenuates below sea level, the inertial navigation system (INS) is generally adopted under water (Titterton and Weston, 2004). Unfortunately, the navigational error of INS tends to accumulate over time. Thus, an aiding system that can mitigate this is required. Such aiding systems mainly used in underwater vehicles include long baseline (LBL), ultra-short baseline (USBL), Doppler velocity log (DVL) and electromagnetic-log (EM-log). Among them, systems such as LBL (Zhang et al., 2018) and USBL (Wang et al., 2020) require a separate infrastructure. On the other hand, DVL (Yao et al., 2017, 2019; Zhu and He, 2020; Hou et al., 2021) and EM-log (Vaisgant et al., 2011; Sun et al., 2015) are equipped in the vehicle's body and are suitable for voyages over long distances. These two sensors are similar in a sense that both provide the vehicle's relative velocity to the sea current to perform the relative navigation, but their principles are quite different.

DVL measures the velocity of the vehicle relative to the ground, which is equal to the absolute velocity, by measuring the Doppler shift of the frequency that occurs when the ultrasonic wave is emitted in the direction of the seabed and returned. Meanwhile, because part of the ultrasonic wave is reflected off the

© The Author(s), 2022. Published by Cambridge University Press on behalf of The Royal Institute of Navigation. This is an Open Access article, distributed under the terms of the Creative Commons Attribution licence (http://creativecommons.org/licenses/by/4.0/), which permits unrestricted re-use, distribution, and reproduction in any medium, provided the original work is properly cited.

https://doi.org/10.1017/S0373463322000431 Published online by Cambridge University Press

underwater float unintentionally, it provides a relative velocity to the sea current rather than the ground velocity: the further the sea floor, the more it captures the velocity relative to the sea current rather than the ground. As DVL intermittently fails to provide any ground velocity, sea current relative navigation using relative velocity to the sea current (Yao et al., 2019) has been studied. On the other hand, EM-log is a device that provides relative velocity to the sea current from induced electromotive force based on Faraday's law. Hence, contrary to DVL, EM-log is not affected by the sea floor and is not detected by other vessels or underwater vehicles.

To use the relative velocity to the sea current as measurement information, it is necessary to model the motion of the sea current. However, it is difficult to model the sea current dynamics because it changes irregularly, depending on various factors, such as wind and temperature. Therefore, in the recent study (Yao et al., 2019), the motion of the sea current was approximated and used as the first-order Markov model (Brown and Hwang, 2012). Nevertheless, since the first-order Markov model consists of only two parameters, there is a limitation in capturing all the dynamics characteristics of the sea current that change every moment. An inaccurate sea current dynamics model degrades the accuracy of navigation; hence, a technique that can compensate for this is required to ensure the success of a prolonged mission.

Therefore, an adaptive filtering technique is required to mitigate the effects of mismodelling the dynamics of the sea current. The adaptive fading extended Kalman filter (AFEKF) is one of such techniques that can compensate for either the inaccurate dynamics model or measurement model of the conventional extended Kalman filter (EKF) using residuals. It has been used in the field of attitude estimation (Johansen and Kristiansen, 2017), topography estimation (Haghighi and Pishkenari, 2021) and fault detection (Kim et al., 2009) as a verified and promising adaptive technique. Still, there has not yet been a precedent of applying the filter in modelling the sea current dynamics.

Another conceivable technique to mitigate the effects of sea current dynamics mismodelling is using multiple models. The interacting multiple model (IMM), originated from the field of target tracking, is the most representative technique that can consider multiple models, and has been widely applied to navigation technology (Cho, 2014; Zhou and Guo, 2018). In particular, in the navigation field of marine vehicles, IMM has been adopted to use multiple measurement models. Yao et al. (2017) has configured an IMM with INS/DVL and zero velocity update (ZUPT), while Yao et al. (2019) and Zhu and He (2020) have proposed an IMM with sub-filters that have different measurement covariance. Nevertheless, these works have overlooked the effects of the mismodelling by simply adopting a single and fixed sea current dynamics model.

In this paper, we propose a method of designing an IMM with AFEKF as sub-filters for the integrated navigation of an underwater vehicle equipped with DVL or EM-log. Despite being more robust than EKF, AFEKF with a single model still has a limited range that the filter can compensate for the inaccurate sea current dynamics models. The composition of the IMM unites the range that each sub-filter can cover, so that performance degradation due to the sea current dynamics mismodelling can be reduced.

The structure of this paper is as follows. Section 2 introduces a general sea current relative navigation method using a single-model EKF. Section 3 introduces a preliminary of adaptive filtering technique to improve the single-model EKF. In Section 4, IMM-AFEKF-based sea current relative navigation method is proposed, and its performance is verified by computer simulation. Finally, Section 5 concludes this paper.

2. Sea current relative navigation

Owing to its accumulating and gradually increasing error over time, INS requires an aiding sensor. In underwater navigation, LBL, USBL, DVL and EM-log are used as such a sensor, but among them, DVL and EM-log do not require additional infrastructure. This section is devoted to illustrating the measurement principle of EM-log and DVL, the sea current dynamics modelling required for their operation and what problems to be overcome when their measurements are used for the integrated navigation.

https://doi.org/10.1017/S0373463322000431 Published online by Cambridge University Press

2.1. EM-log and DVL

EM-log measures the relative velocity of the vehicle to the sea current. Its principle is based on Faraday's law, which states the relationship between induced electromotive force and velocity, shown as Equation (1):

$$E = Bl(v_x - v_{cx}) \tag{1}$$

where E is the electromotive force measured directly by the sensor; B is the strength of the magnetic field; and l is the gap where the induced electromotive force is generated. B and l are calibrated before the use of the sensor; v_x and v_{cx} are the velocity of the vehicle and sea current, respectively, in the x-direction of the vehicle, for example the forward direction. It can be seen that the physical quantity calculated by Equation (1) is not the vehicle's own velocity but its relative velocity to the sea current.

On the other hand, DVL measures the relative velocity of the moving body to the ground, that is the absolute velocity of the vehicle by measuring the Doppler shift, which is the frequency change that occurs when the ultrasonic wave is emitted to the seabed and returned. Equation (2) shows the relationship between the two physical quantities

$$f_0 + \Delta f = \frac{v_u + v}{v_u - v} f_0 \tag{2}$$

where f_0 is original frequency of the emitted ultrasonic wave; v_u is the ultrasonic velocity in water, and Δf and v are the frequency change and the vehicle's velocity, respectively. Generally, since $v_u \gg v$ holds, Equation (2) can be rewritten as Equation (3):

$$v \approx \frac{v_u}{2f_0} \Delta f \tag{3}$$

In other words, there is a linear relationship between the frequency change and the velocity of the vehicle.

However, some of the waves are unintentionally bounced back from the underwater float, providing a relative velocity to the sea current rather than the ground, and the ratio increases as the seabed gets further away. In this case, the velocity should be calculated using Equation (4) instead of Equation (3):

$$v - v_c \approx \frac{v_u}{2f_0} \Delta f \tag{4}$$

Thus, in order to accurately estimate the velocity of the vehicle using EM-log or DVL, the velocity of the sea current must be accurately estimated. This will be dealt with in detail in the following subsection.

2.2. Sea current model

To aid INS using EM-log or DVL, an accurate sea current dynamics model is required. However, as the sea current is affected by countless factors, it is essentially impossible to find a perfect model. Even though there have been various attempts such as advanced three-dimensional circulation model (ADCIRC) (Luettich et al., 1992), curvilinear-grid hydrodynamics 3D (CH3D) (Sheng and Liu, 2011) and regional ocean modelling system (ROMS) (Shchepetkin and McWilliams, 2005) to model the sea current dynamics, it is difficult to implement them in practical applications. A method of preloading the sea current map and using it online has also been researched, but the resolution is limited and the information is insufficient, since the sea current changes every moment.

In this circumstance, it is a reasonable choice to approximate the sea current dynamics model as a first-order Markov model, which has been adopted in the related works (Yao et al., 2019). The first-order

https://doi.org/10.1017/S0373463322000431 Published online by Cambridge University Press

Markov model (Brown and Hwang, 2012) is presented by Equation (5):

$$\dot{v}_c = -\frac{1}{T_c} v_c + w_c \tag{5}$$

where T_c is the time constant, and w_c is the zero-mean white Gaussian noise with standard deviation σ_c. T_c and σ_c are the only two important parameters that describe the first-order Markov process. However, the actual sea current is strongly influenced by topography or wind, ever-changing depending on place and time. In other words, approximating the actual model with a single fixed pair of the parameters has limited effectiveness. Therefore, to overcome this problem, it is desirable to propose a method that adapts each parameter or has several model candidates combining them according to the situation, which is discussed further in Section 3.

2.3. EKF-based sea current relative navigation

One of the most basic methods to implement the sea current relative navigation is to use the conventional EKF. Since the proposed method in this paper also has its roots in an EKF-based method, it is important to note how it is composed. Thus, this subsection is devoted to introducing the conventional EKF-based sea current relative navigation method and its performance evaluation.

2.3.1. Time propagation model

The 15th order INS error model (Titterton and Weston, 2004) is a time propagation model widely used in navigation using inertial sensors. The EKF-based sea current relative navigation augments the sea current velocities in its state vector. The nominal state of the filter is defined in Equation (6):

$$\boldsymbol{x} = \begin{bmatrix} \boldsymbol{p}^T & \boldsymbol{v}^T & \boldsymbol{q}_b^{nT} & \boldsymbol{b}_a^T & \boldsymbol{b}_g^T & \boldsymbol{v}_c^T \end{bmatrix}^T \in \mathbb{R}^{19} \tag{6}$$

where $\boldsymbol{p} = \begin{bmatrix} L & l & h \end{bmatrix}^T$ is the position vector containing latitude, longitude and altitude; $\boldsymbol{v} = \begin{bmatrix} v_N & v_E & v_D \end{bmatrix}^T$ is the velocity vector in the north-east-down (NED) navigation frame $\{n\}$; $\boldsymbol{q}_b^n = \begin{bmatrix} q_0 & q_1 & q_2 & q_3 \end{bmatrix}^T$ is the quaternion between the forward-right-down (FRD) body frame $\{b\}$ and $\{n\}$; and $\boldsymbol{b}_a$ and $\boldsymbol{b}_g$ are the bias of accelerometer and gyro, respectively. Then, the error state vector which is dealt with in the filter is defined in Equation (7):

$$\delta\boldsymbol{x} = \begin{bmatrix} \delta\boldsymbol{p}^T & \delta\boldsymbol{v}^T & \boldsymbol{\varphi}^T & \boldsymbol{b}_a^T & \boldsymbol{b}_g^T & \delta\boldsymbol{v}_c^T \end{bmatrix}^T \in \mathbb{R}^{18} \tag{7}$$

where $\delta\boldsymbol{p}$, $\delta\boldsymbol{v}$, $\boldsymbol{\varphi}$ and $\delta\boldsymbol{v}_c$ are position, velocity, attitude and sea current velocity errors, which are defined as Equation (8), respectively:

$$\begin{aligned} \delta\boldsymbol{p} &= \hat{\boldsymbol{p}} - \boldsymbol{p} \\ \delta\boldsymbol{v} &= \hat{\boldsymbol{v}} - \boldsymbol{v} \\ \boldsymbol{C}(\hat{\boldsymbol{q}}_b^n) &= (\boldsymbol{I}_{3\times3} - [\boldsymbol{\varphi}\times])\boldsymbol{C}(\boldsymbol{q}_b^n) \\ \delta\boldsymbol{v}_c &= \hat{\boldsymbol{v}}_c - \boldsymbol{v}_c \end{aligned} \tag{8}$$

where the $\hat{\cdot}$ symbol indicates the estimates of the symbol right below; $\boldsymbol{C}(\boldsymbol{q})$ is a direction cosine matrix corresponding to $\boldsymbol{q}$; and $[\cdot\times]$ transforms vector in $\mathbb{R}^3$ to a skew symmetric matrix.

The sea current-augmented INS model for the state vector in Equation (6) is presented in Equation (9):

$$\dot{\boldsymbol{x}} = f(\boldsymbol{x}, \boldsymbol{u}, \boldsymbol{w}_c) \tag{9}$$

https://doi.org/10.1017/S0373463322000431 Published online by Cambridge University Press

where $\boldsymbol{u}$ indicates the inertial measurement vector. Then, Equation (10) is obtained by linearisation of Equation (9) for $\delta\boldsymbol{x}$:

$$\begin{aligned}\delta\dot{\boldsymbol{x}} &= \boldsymbol{F}\delta\boldsymbol{x} + \boldsymbol{w}\\ &= \begin{bmatrix}\boldsymbol{F}_{pp} & \boldsymbol{F}_{pv} & \boldsymbol{0}_{3\times3} & \boldsymbol{0}_{3\times3} & \boldsymbol{0}_{3\times3} & \boldsymbol{0}_{3\times3}\\ \boldsymbol{F}_{vp} & \boldsymbol{F}_{vv} & \boldsymbol{F}_{v\varphi} & \boldsymbol{F}_{vb} & \boldsymbol{0}_{3\times3} & \boldsymbol{0}_{3\times3}\\ \boldsymbol{F}_{\varphi p} & \boldsymbol{F}_{\varphi v} & \boldsymbol{F}_{\varphi\varphi} & \boldsymbol{0}_{3\times3} & \boldsymbol{F}_{\varphi b} & \boldsymbol{0}_{3\times3}\\ \boldsymbol{0}_{3\times3} & \boldsymbol{0}_{3\times3} & \boldsymbol{0}_{3\times3} & \boldsymbol{0}_{3\times3} & \boldsymbol{0}_{3\times3} & \boldsymbol{0}_{3\times3}\\ \boldsymbol{0}_{3\times3} & \boldsymbol{0}_{3\times3} & \boldsymbol{0}_{3\times3} & \boldsymbol{0}_{3\times3} & \boldsymbol{0}_{3\times3} & \boldsymbol{0}_{3\times3}\\ \boldsymbol{0}_{3\times3} & \boldsymbol{0}_{3\times3} & \boldsymbol{0}_{3\times3} & \boldsymbol{0}_{3\times3} & \boldsymbol{0}_{3\times3} & \boldsymbol{F}_{cc}\end{bmatrix}\delta\boldsymbol{x} + \begin{bmatrix}\boldsymbol{0}_{3\times1}\\ \boldsymbol{w}_a\\ \boldsymbol{w}_g\\ \boldsymbol{0}_{3\times1}\\ \boldsymbol{0}_{3\times1}\\ \boldsymbol{w}_c\end{bmatrix}\end{aligned} \tag{10}$$

where $\boldsymbol{w}_a$ and $\boldsymbol{w}_g$ are the zero-mean white Gaussian noise of the accelerometer and gyro, respectively, of which covariances are nominated by $\boldsymbol{Q}_a$ and $\boldsymbol{Q}_g$. The submatrices in Equation (10) are presented in Appendix A, and the detailed derivation process is introduced in Titterton and Weston (2004).

2.3.2. Measurement update model

EM-log or DVL provide velocity information relative to the sea current, as discussed in Section 2. Hence, the measurement model for them is expressed as Equation (11):

$$\begin{aligned}\boldsymbol{\rho} &= \hat{\boldsymbol{C}}_n^b(\hat{\boldsymbol{v}} - \hat{\boldsymbol{v}}_{\boldsymbol{c}}) - \boldsymbol{z}\\ &\approx \begin{bmatrix}\boldsymbol{0}_{3\times3} & \boldsymbol{C}_n^b & -\boldsymbol{C}_n^b[(\boldsymbol{v} - \boldsymbol{v}_{\boldsymbol{c}})\times] & \boldsymbol{0}_{3\times3} & \boldsymbol{0}_{3\times3} & -\boldsymbol{C}_n^b\end{bmatrix}\delta\boldsymbol{x} + \boldsymbol{\eta}\\ &:= \boldsymbol{H}\delta\boldsymbol{x} + \boldsymbol{\eta}\end{aligned} \tag{11}$$

where $\boldsymbol{z}$ is the velocity measurement of EM-log or DV;, and $\boldsymbol{\eta}$ is the zero-mean white Gaussian noise with covariance $\boldsymbol{R}$. Note that Equation (11) generates a correlation between the INS error and the sea current which are independent at time propagation process as shown in Equation (10). In other words, if the parameters of the sea current propagation model dealt with in Equation (5) are not correct, it will adversely affect the navigation error in the measurement update process.

3. Adaptive filtering preliminary to sea current relative navigation

The sea current relative navigation requires a dynamics model of the sea currents. However, since the conventional method uses a single fixed model, as in Equation (5), the navigation performance is degraded due to mismodelling of the true sea current. To overcome this problem, two adaptive techniques are applied in this paper: one is an adaptive fading technique (Kim et al., 2009) that compensates for the effects of sea current parameter modelling errors online, and the other is the IMM technique (Yao et al., 2017, 2019; Zhu and He, 2020) that uses two or more models in combination.

3.1. Adaptive fading extended Kalman filter

The AFEKF compensates for model inaccuracy by comparing the filter residual and its covariance. The model inaccuracy is inherent in the time propagation model or the measurement update model. Depending on where the inaccuracy exists, the AFEKF applies the adaptive technique by using the two forgetting factors β_k and γ_k in different ways.

First, in the filter, the calculated residual covariance is obtained as in Equation (14):

$$\boldsymbol{S}_k = \boldsymbol{H}_k\boldsymbol{P}_k^-\boldsymbol{H}_k^T + \boldsymbol{R}_k \tag{14}$$

https://doi.org/10.1017/S0373463322000431 Published online by Cambridge University Press

On the other hand, the estimated residual covariance is obtained using the sampled residuals $\boldsymbol{\rho}_i$ as in Equation (15):

$$\bar{\boldsymbol{S}}_k = \frac{1}{M-1} \sum_{i=k-M+1}^{k} \boldsymbol{\rho}_i \boldsymbol{\rho}_i^T \tag{15}$$

where M is the fading window size, and $\boldsymbol{P}_k^-$ is *a priori* covariance. By comparing these two covariances as in Equation (16), the forgetting factor β_k is obtained:

$$\beta_k = \max\left\{1, \frac{1}{m}\text{trace}(\bar{\boldsymbol{S}}_k \boldsymbol{S}_k^{-1})\right\} \text{ OR } \beta_k = \max\{1, \text{trace}(\bar{\boldsymbol{S}}_k)/\text{trace}(\boldsymbol{S}_k))\} \tag{16}$$

where m is the dimension of the measurement vector; γ_k adjusts the *a priori* covariance and Kalman gain together with another forgetting factor β_k, as in Equation (17):

$$\begin{aligned} \bar{\boldsymbol{P}}_k^- &= \gamma_k \boldsymbol{P}_k^- \\ \bar{\boldsymbol{K}}_k &= \frac{\gamma_k}{\beta_k} \bar{\boldsymbol{P}}_k^- \boldsymbol{H}_k^T (\boldsymbol{H}_k \bar{\boldsymbol{P}}_k^- \boldsymbol{H}_k^T + \boldsymbol{R}_k)^{-1} \end{aligned} \tag{17}$$

As mentioned previously, AFEKF is implemented differently according to the model inaccuracies. If the time propagation model is inaccurate, γ_k is set as β_k, so that it inflates *a priori* covariance but does not particularly adjust the Kalman gain. In contrast, if the measurement update model is inaccurate, γ_k is set as 1, so that the update rate is reduced by adjusting the Kalman gain. Our problem falls under the former case since the propagation model of the sea current is inaccurate.

3.2. Interacting multiple model

IMM was initially applied and used in the field of target tracking. Since the dynamics model of a target is not precisely known, generally, several manoeuvre candidates are modelled as sub-filters, and the transition probability between them is reflected in IMM. After successful application in the field of target tracking, it has been widely used in the field of navigation. In particular, in the navigation field of marine vehicles, there are cases such as using different types of measurement (Yao et al., 2017) or setting different measurement covariance in each sub-filter (Yao et al., 2019; Zhu and He, 2020). Nevertheless, they do not focus on the modelling of the sea current dynamics, which is one of the most important aspects in sea current relative navigation. In this paper, therefore, the sea current relative navigation is performed using multiple sub-filters with different sea current dynamics models.

Figure 1 shows the sea current relative navigation scheme using the IMM filter. To operate an IMM, first, it is necessary to define the Markov chain transition matrix $\boldsymbol{T}$, which deals with the transition probability between the sea current models in each sub-filter. In this paper, two sub-filters, that is, two model candidates, are used for convenience, and the transition matrix is defined as Equation (18):

$$\boldsymbol{T} = \begin{bmatrix} p_{11} & p_{12} \\ p_{21} & p_{22} \end{bmatrix} \tag{18}$$

where each element of $\boldsymbol{T}$, $p_{ij} := \Pr(\alpha_k = j | \alpha_{k-1} = i)$ represents the probability that the sea current model α changes from i-th model at the previous time step $t = k-1$ to j-th model at the current time step $t = k$, and hence, the sum of each row of $\boldsymbol{T}$, $p_{i1} + p_{i2} = 1$ must be satisfied, accordingly. In addition, the mode probability vector $\boldsymbol{\mu}_k$, which indicates the probability of following a certain sub-filter model, is defined as Equation (19):

$$\boldsymbol{\mu}_k = \begin{bmatrix} \mu_{1,k} & \mu_{2,k} \end{bmatrix}^{\boldsymbol{T}} \tag{19}$$

https://doi.org/10.1017/S0373463322000431 Published online by Cambridge University Press

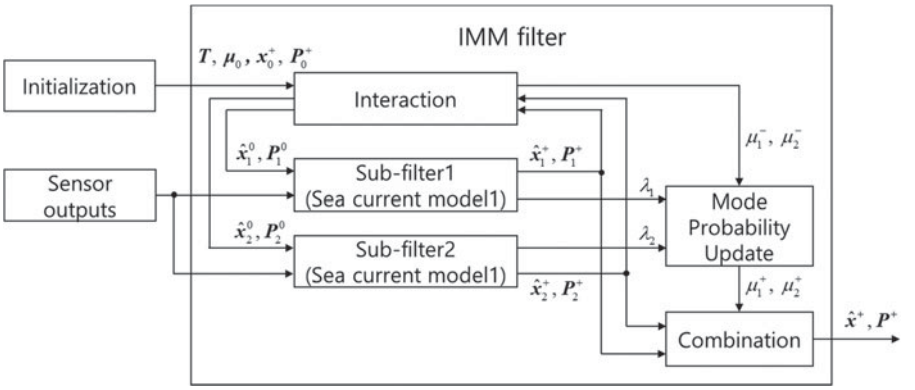

Figure 1. *IMM filter structure for sea current relative navigation.*

where $\mu_{j,k}$ is the mode probability of the j-th sub-filter at $t = k$, and it must satisfy $\mu_{1,k} + \mu_{2,k} = 1$, which initial value is given as $\boldsymbol{\mu}_0^+$. The IMM filter has an iterative configuration of the following four steps with predefined $\boldsymbol{T}$ and $\boldsymbol{\mu}_0^+$.

3.2.1. Interaction

In the first step, also called the mixing probability process, the state variable, covariance and mode probability to be handled in each sub-filter of the current time step are initialised from the results of the previous time step. First, the mode probability is propagated as in Equation (20) using the transition matrix of Equation (18):

$$\mu_{j,k}^- := \Pr(\alpha_k = j | \boldsymbol{Z}_{1:k-1}^*) = \sum_{i=1}^{2} p_{ij} \mu_{i,k-1}^+ \tag{20}$$

where $\boldsymbol{Z}_{1:k-1}^*=\{z_1, \cdots, z_{k-1}\}$ is a set of measurements up to the previous time step, so that the mode probability $\mu_{j,k}^-$ of Equation (20) contains information of measurements up to the previous time step. Next, the mixing probability is calculated as in Equation (21) according to Bayes' rule:

$$\mu_{i|j,k-1} := \Pr(\alpha_{k-1} = i | \alpha_k = j) = \frac{p_{ij} \mu_{i,k-1}^+}{\mu_{j,k}^-} \tag{21}$$

Using Equation (21), the state variable and covariance to be estimated in each sub-filter is initialised as Equation (22):

$$\begin{aligned} \hat{\boldsymbol{x}}_{j,k-1}^0 &:= \mathrm{E}\left[\boldsymbol{x}_{k-1} | \alpha_k = j, \boldsymbol{Z}_{1:k-1}^*\right] = \sum_{i=1}^{2} \hat{\boldsymbol{x}}_{i,k-1}^+ \mu_{i|j,k-1} \\ \boldsymbol{P}_{j,k-1}^0 &:= E\left[(\boldsymbol{x}_{k-1} - \hat{\boldsymbol{x}}_{j,k-1}^0)(\boldsymbol{x}_{k-1} - \hat{\boldsymbol{x}}_{j,k-1}^0)^T | \alpha_k = j, \boldsymbol{Z}_{1:k-1}^*\right] \\ &= \sum_{i=1}^{2} \{\boldsymbol{P}_{i,k-1}^+ + (\hat{\boldsymbol{x}}_{i,k-1}^+ - \hat{\boldsymbol{x}}_{j,k-1}^0)(\hat{\boldsymbol{x}}_{i,k-1}^+ - \hat{\boldsymbol{x}}_{j,k-1}^0)^T\} \mu_{i|j,k-1}^+ \end{aligned} \tag{22}$$

3.2.2. Sub-filtering

In the second step, the time propagation and measurement update are performed in each sub-filter according to its own models. At this step, the model or the type of sub-filters should be different from

https://doi.org/10.1017/S0373463322000431 Published online by Cambridge University Press

each other. The sub-filtering is summarised as:

$$\begin{aligned}
\hat{\boldsymbol{x}}^{-}_{j,k} &:= \mathrm{E}\left[\boldsymbol{x}_k|\alpha_k = j, \boldsymbol{Z}^{*}_{1:k-1}\right] = f(\hat{\boldsymbol{x}}^{0}_{j,k-1}, \boldsymbol{u}_k)\\
\boldsymbol{P}^{-}_{j,k} &:= E\left[(\boldsymbol{x}_k - \hat{\boldsymbol{x}}^{-}_{j,k})(\boldsymbol{x}_k - \hat{\boldsymbol{x}}^{-}_{j,k})^T|\alpha_k = j, \boldsymbol{Z}^{*}_{1:k-1}\right] = \boldsymbol{F}_{j,k}\boldsymbol{P}^{0}_{j,k-1}\boldsymbol{F}^{T}_{j,k} + \boldsymbol{Q}_{j,k}\\
\boldsymbol{K}_{j,k} &= \boldsymbol{P}^{-}_{j,k}\boldsymbol{H}_{j,k}\boldsymbol{S}^{-1}_{j,k}\\
\hat{\boldsymbol{x}}^{+}_{j,k} &:= \mathrm{E}\left[\boldsymbol{x}_k|\alpha_k = j, \boldsymbol{Z}^{*}_{1:k}\right] = \hat{\boldsymbol{x}}^{-}_{j,k} + \boldsymbol{K}_{j,k}\boldsymbol{\rho}_{j,k}\\
\boldsymbol{P}^{+}_{j,k} &:= E\left[(\boldsymbol{x}_k - \hat{\boldsymbol{x}}^{+}_{j,k})(\boldsymbol{x}_k - \hat{\boldsymbol{x}}^{+}_{j,k})^T|\alpha_k = j, \boldsymbol{Z}^{*}_{1:k}\right] = (\boldsymbol{I} - \boldsymbol{K}_{j,k}\boldsymbol{H}_{j,k})\boldsymbol{P}^{-}_{j,k}
\end{aligned} \tag{23}$$

3.2.3. Mode probability calculation

In the third step, the mode probability of each sub-filter is updated. It is based on the likelihood of the residual, which is calculated in each sub-filter as shown in Equation (24):

$$\lambda_{j,k} = \frac{1}{\sqrt{\det(2\pi \boldsymbol{S}_{j,k})}} exp\left\{-\frac{1}{2}\boldsymbol{\rho}^{T}_{j,k}\boldsymbol{S}^{-1}_{j,k}\boldsymbol{\rho}_{j,k}\right\} \tag{24}$$

Bayes' rule and Equation (24) lead to Equation (25), which contains the information of the measurement of the current time step in the mode probability of each sub-filter:

$$\mu^{+}_{j,k} := \Pr(\alpha_k = j|\boldsymbol{Z}^{*}_{k}) = \frac{\lambda_{j,k}\mu^{-}_{j,k}}{\sum_{i=1}^{2}\lambda_{i,k}\mu^{-}_{i,k}} \tag{25}$$

3.2.4. Combination of estimation

In the last step, the final solution of the IMM filter is calculated by combining the result of each sub-filter as:

$$\begin{aligned}
\hat{\boldsymbol{x}}^{+}_{k} &= \sum_{j=1}^{2}\hat{\boldsymbol{x}}^{+}_{j,k}\mu^{+}_{j,k}\\
\boldsymbol{P}^{+}_{k} &= \sum_{j=1}^{2}\{\boldsymbol{P}^{+}_{j,k} + (\hat{\boldsymbol{x}}^{+}_{j,k} - \hat{\boldsymbol{x}}^{+}_{k})(\hat{\boldsymbol{x}}^{+}_{j,k} - \hat{\boldsymbol{x}}^{+}_{k})^T\}\mu^{+}_{j,k}
\end{aligned} \tag{26}$$

To improve the performance of the sea current relative navigation, the IMM filter is configured by sub-filters with different sea current dynamics models, thus adopting the one that best describes the actual sea current dynamics. The filter can be designed by adjusting the transition matrix as well as the sea current parameters $T_{c,i}$ and $\sigma_{c,i}$.

4. IMM-AFEKF-based sea current relative navigation

In this section, we propose an IMM–AFEKF-based sea current relative navigation method that combines the adaptive fading method that adjusts the sea current model parameters and IMM using multiple sea currents models, to improve the navigation performance. The results demonstrate a performance improvement from applying the adaptive fading technique to the conventional EKF in situations where the sea current dynamics model is inaccurate. Then, the limitation of a single model-based method is analysed, which is overcome by configuring a multiple model structure using IMM.

4.1. Filter configuration

IMM–AFEKF-based sea current relative navigation has a similar structure to an IMM-based method, shown in Figure 1, with a difference in equipping its sub-filters with AFEKFs of different sea current

https://doi.org/10.1017/S0373463322000431 Published online by Cambridge University Press

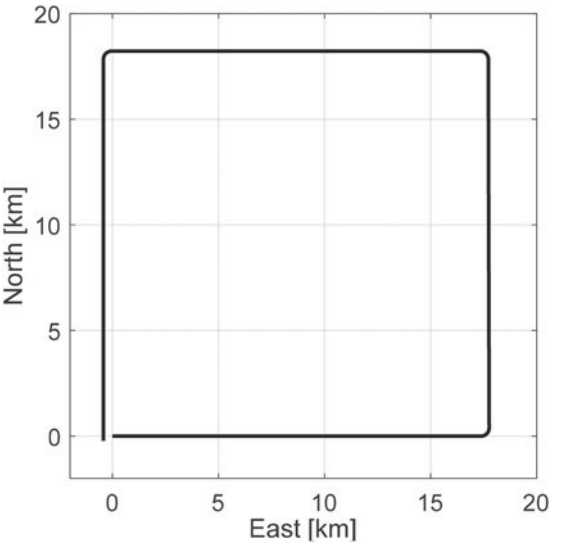

Figure 2. *Simulation trajectory.*

Table 1. *Sensor specification.*

	Accelerometer	Gyro	EM-log/DVL
Bias	$0 \cdot 05$ mg	$0 \cdot 02$ deg/h	–
Noise	$0 \cdot 01$ mg/$\sqrt{\text{Hz}}$	$0 \cdot 005$ deg/$\sqrt{\text{hr}}$	$0 \cdot 01$ m/s
Sampling rate	100 Hz		1 Hz

parameters. The window size M is set to 20. Among the two parameters T_c and σ_c that configure the sea current model approximated by first-order Markov process, the latter further affects filter performance. Hence, $T_{c,1} = T_{c,2} = 2$ h is fixed and let $\sigma_{c,1} < \sigma_{c,2}$ for convenience. Meanwhile, since the conversion between sea current models does not occur frequently, $\boldsymbol{T} = \begin{bmatrix} 0 \cdot 9 & 0 \cdot 1 \\ 0 \cdot 1 & 0 \cdot 9 \end{bmatrix}$ is set. Also, the initial mode probability is set to $\boldsymbol{\mu}_0^+ = \begin{bmatrix} 0 \cdot 5 & 0 \cdot 5 \end{bmatrix}^T$ since initial information about the sea current model is insufficient, in general.

4.2. Performance evaluation

4.2.1. Conventional method

To show the performance degradation caused by an inaccurate sea current model in conventional EKF-based sea current relative navigation, a simulation was performed. The trajectory used in the simulation is as shown in Figure 2, where the vehicle moves counter-clockwise for 2 h at a constant speed of 20 knots from the origin of 36 degrees north latitude and 127 degrees east longitude. The sensor specifications were set as shown in Table 1, and measurements of EM-log or DVL in the forward direction of the body frame were used for convenience.

Figure 3 shows the performance degradation due to an inaccurate sea current model when performing EKF-based sea current relative navigation. The x-axis of the figure is the actual σ_c used to generate the sea current data, which is denoted by σ_t in this paper to distinguish it from σ_f used in the filter model. According to a survey by the Korea Hydrographic and Oceanographic Agency, the sea current speed near the Korean Peninsula is generally less than 1 kn, so it was carried out up to σ_t of 1 m/s with

https://doi.org/10.1017/S0373463322000431 Published online by Cambridge University Press

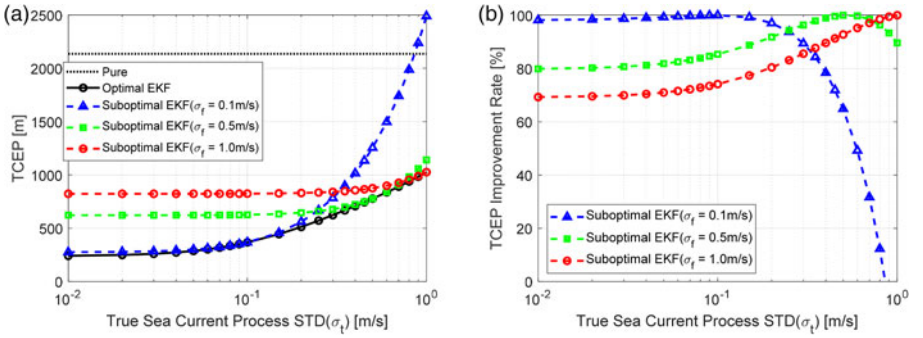

Figure 3. *Performance of EKF-based sea current relative navigation with incorrect parameters. (a) TCEP, (b) TCEP compared to optimal filter.*

a margin. The y-axes of (a) and (b) of Figure 3 are the time circular error probable (TCEP) and its improvement rate after 2 h navigation, respectively. TCEP is defined as Equation (27):

$$\mathrm{TCEP}_k = 0 \cdot 589 \times \{\mathrm{RMS}(\delta P_{N,1:k}) + \mathrm{RMS}(\delta P_{E,1:k})\} \tag{27}$$

where k is the current time step, and RMS stands for root mean squares. The reason for adopting such TCEP index is that it can reduce the effect of the Schuler period (Titterton and Weston, 2004), which appears in general indices such as RMS error and CEP. The black dotted line is the result of performing the pure navigation without the measurement update, and the circle-marked black solid line is the minimum error which can be achieved when synchronously setting σ_f with σ_t in an EKF-based sea current relative navigation, hence indicating an optimal result. Finally, the triangle-marked blue line, the square-marked green line, and the diamond-marked red line are the results of σ_f is set by $0 \cdot 1, 0 \cdot 5$ and $1 \cdot 0$ m/s, respectively, regardless of σ_t, representing suboptimal results. Each point represents 100 times of Monte-Carlo simulation result, where the other parameter of the sea current model, T_c, was fixed as 2 h.

As expected, the pure navigation results in Figure 3(a) shows constant performance regardless of sea current model since it does not use Equation (11). In contrast, in the case of the optimal EKF, the performance deteriorates as the standard deviation of the sea current increases, which is further elaborated in Appendix B. The TCEPs of suboptimal EKF are the same with those of the optimal EKF at $\sigma_f = \sigma_t$ and larger elsewhere. Note that the performance degradation is particularly greater where $\sigma_t > \sigma_f$ than in the opposite case, and when $\sigma_t \gg \sigma_f$, the performance of EKF-based sea current relative navigation is inferior to that of the pure navigation.

Figure 3(b) shows the result of suboptimal EKF shown in Figure 3(a) compared with the results of pure navigation and optimal EKF, presented through a converted TCEP value, shown in Equation (28):

$$\mathrm{TCEP\,rate} = \frac{\mathrm{TCEP}_{\mathrm{pure}} - \mathrm{TCEP}_{\mathrm{sub}}}{\mathrm{TCEP}_{\mathrm{pure}} - \mathrm{TCEP}_{\mathrm{opt}}} \times 100\% \tag{28}$$

This index shows how much the performance of the suboptimal EKF is degraded by sea current mismodelling compared to the optimal performance improvement that can be achieved by the aiding sensors. The figure also shows that the performance improvement is more degraded when $\sigma_t > \sigma_f$, and if $\sigma_t \gg \sigma_f$, the performance improvement of EKF-based sea current relative navigation becomes negative.

To sum up, the EKF-based sea current relative navigation can show optimal performance only when the current parameters are correctly set, which is practically impossible to be satisfied, and the performance cannot be guaranteed with a single fixed parameter. Therefore, a novel method using adaptive techniques is required for the sea current relative navigation with guaranteed performance.

https://doi.org/10.1017/S0373463322000431 Published online by Cambridge University Press

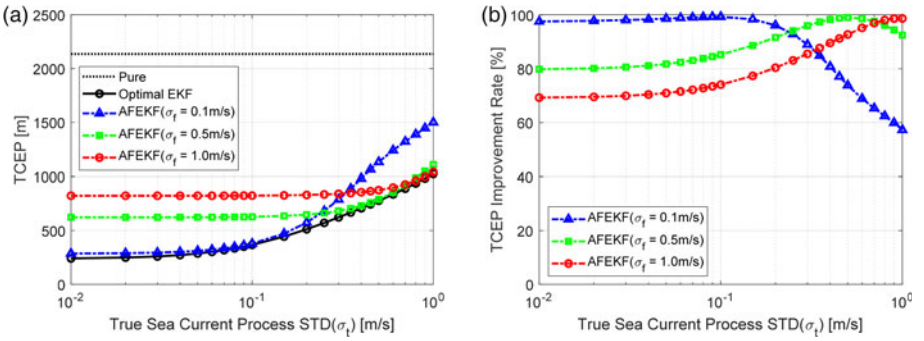

Figure 4. *Performance of AFEKF-based sea current relative navigation with incorrect parameters. (a) TCEP, (b) TCEP compared to optimal filter.*

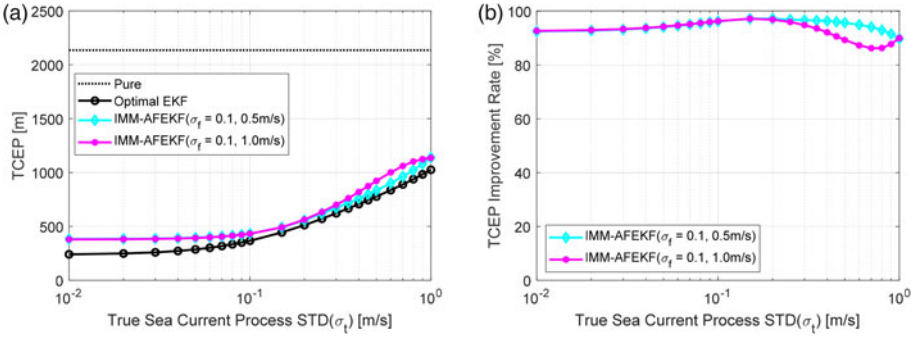

Figure 5. *Performance of IMM-AFEKF-based sea current relative navigation with multiple parameters. (a) TCEP, (b) TCEP compared to optimal filter.*

4.2.2. Proposed method

To verify the performance of the proposed method, a new simulation was performed by replacing the conventional fixed single-model EKF with a single-model AFEKF under the same conditions as the simulation performed in Section 2. Figure 4 shows the navigation performance of a single AFEKF compared to the results of the pure navigation and optimal EKF-based sea current relative navigation. Compared with the conventional EKF results in Figure 3, it can be seen that the degradation of navigation performance is reduced in the large σ_t domain. Nevertheless, none of the single model AFEKFs shows a prominent performance in the entire σ_t domain. In other words, similarly to the EKF, when σ_f is set small, a prominent performance is shown in the domain where σ_t is also small, but performance degradation occurs in the domain where σ_t is large indeed. Similarly, when σ_f is set large, the opposite is true for σ_t values.

Based on such insight, an additional simulation was performed to verify the performance of IMM–AFEKF, of which the results are shown in Figure 5. Two AFEKFs from the simulations shown in Figure 4 are adopted as sub-filters of IMM–AFEKF. In particular, the first sub-filter was fixed to $\sigma_{f,1} = 0 \cdot 1$ m/s in order to guarantee the performance in the small σ_t domain. From this simulation, it was confirmed that the performance of the IMM–AFEKF was more robust than the single models, maintaining high TCEP improvement of 90% rate in all σ_t domain. In addition, in the domain of $0 \cdot 1 < \sigma_t < 1 \cdot 0$ m/s, the IMM filter with $\sigma_{f,2} = 0 \cdot 5$ m/s has a better performance than that with $\sigma_{f,2} = 1 \cdot 0$ m/s due to the adaptive fading scheme.

Tables 2 and 3 show the navigation results of chosen filters at $\sigma_t = 0 \cdot 05$ m/s and $\sigma_t = 1$ m/s as representatives of the small σ_t domain and the large σ_t domain, respectively. It was confirmed that the results were consistent with the previous analysis. When σ_t is small, as detailed in Table 2, it can be seen

https://doi.org/10.1017/S0373463322000431 Published online by Cambridge University Press

Table 2. *Navigation performance of various filters in small σ_t domain (0·05 m/s).*

Filter	Position error [m]	Velocity error [m/s]	Levelling error [deg]	Heading error [deg]
EKF ($\sigma_f = 0 \cdot 1$ m/s)	362	0·411	0·00353	0·0221
AFEKF ($\sigma_f = 0 \cdot 1$ m/s)	375	0·418	0·00361	0·0222
EKF ($\sigma_f = 0 \cdot 5$ m/s)	749	0·483	0·00421	0·0241
AFEKF ($\sigma_f = 0 \cdot 5$ m/s)	750	0·485	0·00424	0·0241
IMM-AFEKF ($\sigma_f = 0 \cdot 1,\ \ 0 \cdot 5$ m/s)	477	0·435	0·00374	0·0228

Table 3. *Navigation performance of various filters in large σ_t domain (1 m/s).*

Filter	Position error [m]	Velocity error [m/s]	Levelling error [deg]	Heading error [deg]
EKF ($\sigma_f = 0 \cdot 1$ m/s)	2990	1·41	0·0119	0·0511
AFEKF ($\sigma_f = 0 \cdot 1$ m/s)	1820	0·998	0·00770	0·0285
EKF ($\sigma_f = 0 \cdot 5$ m/s)	1370	0·889	0·00712	0·0263
AFEKF ($\sigma_f = 0 \cdot 5$ m/s)	1330	0·888	0·00695	0·0255
IMM-AFEKF ($\sigma_f = 0 \cdot 1,\ \ 0 \cdot 5$ m/s)	1370	0·905	0·00716	0·0257

that the navigation errors of single model filters with small σ_f are satisfactory. Note that the EKF-based ones show slightly better performance than do the AFEKF-based ones, because the adaptive fading technique can only inflate the overestimated *a priori* covariance but cannot deflate the underestimated one, as shown in Equations (16) and (17). However, as detailed in Table 3, the performance of those single-model filters with small σ_f rapidly deteriorates in the region where σ_t is large. In particular, the EKF-based one shows severe performance degradation due to its incapability to compensate for the inaccurate sea current dynamics model. On the contrary, single-model filters with large σ_f have decent performance in the large σ_t domain but deteriorate in the region where σ_t is small. Still, the adaptive fading technique is effective for cases when $\sigma_f < \sigma_t$, as in Table 3. Finally, the proposed IMM–AFEKF filter shows the most robust navigation performance in all domains of σ_t. Due to the influence of the sub-filter of the relatively inaccurate model, the proposed method presents slightly worse performance compared to the best filter. Nonetheless, we would like to point out once again the high TCEP rate of over 90% shown in Figure 5(b), and safely claim that the performance discrepancy between the proposed and the best is insignificant.

Notice that the filter that performs best in one case has the worst performance in the other case, indicating that single-model filters lack reliability. Thus, the proposed method is most suitable for the sea current relative navigation where σ_t is uncertain.

Figure 6 shows the mode probability from the simulation shown in Figure 5. In the domain where σ_t is small, the model of sub-filter 1 is more similar to the actual model, hence the mode probability is high and, conversely, the mode probability of sub-filter 1 decreases rapidly in the domain where σ_t is large. Note that since the sum of the mode probabilities of all sub-filters must be 1 in each IMM, as one mode probability decreases, the other increases accordingly. In addition, it was confirmed that the greater the difference between $\sigma_{f,1}$ and $\sigma_{f,2}$, the greater the difference of mode probabilities. As a result, in the σ_t domain where the performance of one sub-filter is degraded, the other sub-filter compensates for it, thereby improving the integrated navigation performance.

From this analysis, the proposed IMM-AFEKF-based sea current relative navigation may be unsuitable in the case when strong prior information about the sea current velocity is given. In other words, it may be more appropriate to use a specific single filter when changes of the sea current velocity can

https://doi.org/10.1017/S0373463322000431 Published online by Cambridge University Press

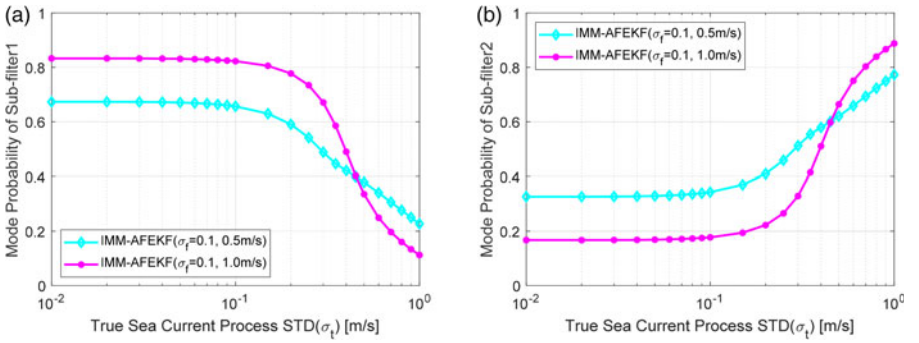

Figure 6. *Mode probability of IMM-AFEKF-based sea current relative navigation with multiple parameters. (a) Sub-filter 1, (b) Sub-filter 2.*

be predicted accurately in the area to be navigated. In addition, the computation complexity is naturally increased when compared to those of the existing filters. However, if sub-filtering is implemented well in parallel, this problem can be alleviated. Also, since the adaptive fading scheme is one of many components of the overall structure, the increased computational cost should not be a major concern in implementing the proposed method. As a future work, it is possible to improve the transition probability matrix, a key element in designing IMM.

5. Conclusion

In this paper, a sea current relative navigation method using an IMM–AFEKF scheme is proposed. An accurate sea current dynamics model is required to perform the relative navigation to the sea current. Yet, describing the true sea current dynamics is near impossible in practice. Therefore, an IMM filter using multiple model candidates and an adaptive fading technique that can compensate for the inaccuracy of each model is adopted. The performance of the conventional EKF-based sea current relative navigation deteriorated when the standard deviation of sea current approximated by the first-order Markov model was smaller than actual value. Although the performance degradation was reduced when the adaptive fading technique was applied, there was a limit to the sea current domain where the navigation performance is guaranteed with the single filter. In contrast, the IMM–AFEKF-based sea current relative navigation method proposed in this paper showed good performance in the entire domain as one sub-filter compensated for the performance degradation of the other. In particular, due to the adaptive fading scheme, it showed superior performance even when the standard deviations of the sub-filters were set smaller than the actual value. Eventually, it was possible to guarantee more than 90% of the performance compared to the optimal EKF-based sea current relative navigation. It was found that the proposed method requires more computation, but the computation time of IMM, which greatly contributes to such increase, can be reduced through sub-filtering in parallel. In addition, it is expected that a more meticulously designed transition probability matrix will improve the filter performance.

Funding statement. This research was supported in part by Hanwha Corp., and Unmanned Vehicles Core Technology Research and Development Program through the National Research Foundation of Korea (NRF), Unmanned Vehicle Advanced Research Center (UVARC) funded by the Ministry of Science and ICT, the Republic of Korea (No. NRF-2020M3C1C1A01086408).

References

Brown, R. G. and Hwang, P. Y. C. (2012). *Introduction to Random Signals and Applied Kalman Filtering: With MATLAB Exercises*. New York: Wiley & Sons.

Cho, S. Y. (2014). IM-Filter for INS/GPS-integrated navigation system containing low-cost gyros. *IEEE Transactions on Aerospace and Electronic Systems*, **50**, 2619–2629.

Groves, P. D. (2013). *Principles of GNSS, Inertial, and Multisensor Integrated Navigation Systems*. Boston: Artech House.

https://doi.org/10.1017/S0373463322000431 Published online by Cambridge University Press

Haghighi, M. S. and Pishkenari, H. N. (2021). Real-time topography and Hamaker constant estimation in atomic force microscopy based on adaptive fading extended Kalman filter. *International Journal of Control Automation and Systems*, **19**, 2455–2467.

Hou, L. H., Xu, X. S., Yao, Y. Q., Wang, D. and Tong, J. W. (2021). Improved exponential weighted moving average based measurement noise estimation for strapdown inertial navigation system/Doppler velocity log integrated system. *The Journal of Navigation*, **74**, 467–487.

Johansen, T.-A. and Kristiansen, R. (2017). Quadrotor Attitude Estimation Using Adaptive Fading Multiplicative EKF. *Proceedings of the 2017 American Control Conference*, Seattle, WA.

Kim, K. H., Lee, J. G. and Park, C. G. (2009). Adaptive two-stage extended Kalman filter for a fault-tolerant INS-GPS loosely coupled system. *IEEE Transactions on Aerospace and Electronic Systems*, **45**, 125–137.

Luettich, R. A., Westerink, J. J. and Scheffner, N. W. (1992) ADCIRC: an advanced three-dimensional circulation model for shelves, coasts, and estuaries. Report 1, Theory and methodology of ADCIRC-2DD1 and ADCIRC-3DL. *Dredging Research Program Technical Report*, DRP-92-6. US Army Corps of Engineering, Washington, DC.

Shchepetkin, A. F. and McWilliams, J. C. (2005). The regional oceanic modeling system (ROMS): A split-explicit, free-surface, topography-following-coordinate oceanic model. *Ocean Modelling*, **9**, 347–404.

Sheng, Y. P. and Liu, T. (2011). Three-dimensional simulation of wave-induced circulation: Comparison of three radiation stress formulations. *Journal of Geophysical Research: Oceans*, **115**, C05021.

Sun, F., Xia, J. Z., Ben, Y. Y. and Zu, Y. (2015). A novel EM-Log aided gyrocompass alignment for in-motion marine SINS. *Optik*, **126**, 2099–2103.

Titterton, D. H. and Weston, J. L. (2004). *Strapdown Inertial Navigation Technology*. Reston, VA Stevenage, UK: American Institute of Aeronautics and Astronautics; Institution of Electrical Engineers.

Vaisgant, I., Litvinenko, Y. A. and Tupysev, V. (2011). Verification of EM log data in marine inertial navigation system correction. *Gyroscopy and Navigation*, **2**, 34–38.

Wang, J., Zhang, T., Jin, B. N., Zhu, Y. Y. and Tong, J. W. (2020). Student's t-based robust Kalman filter for a SINS/USBL integration navigation strategy. *IEEE Sensors Journal*, **20**, 5540–5553.

Yao, Y. Q., Xu, X. S. and Xu, X. (2017). An IMM-aided ZUPT methodology for an INS/DVL integrated navigation system. *Sensors*, **17**, 2030.

Yao, Y. Q., Xu, X. S., Li, Y. and Zhang, T. (2019). A hybrid IMM based INS/DVL integration solution for underwater vehicles. *IEEE Transactions on Vehicular Technology*, **68**, 5459–5470.

Zhang, T., Chen, L. P. and Yan, Y. X. (2018). Underwater positioning algorithm based on SINS/LBL integrated system. *IEEE Access*, **6**, 7157–7163.

Zhou, D. P. and Guo, L. (2018). A DDF-based IMM-TFS approach for the accuracy evaluation problem of rapid transfer alignment. *The Journal of Navigation*, **71**, 749–768.

Zhu, B. and He, H. Y. (2020). Integrated navigation for Doppler velocity log aided strapdown inertial navigation system based on robust IMM algorithm. *Optik*, **217**, 164871.

A. Appendix A: 15th order inertial navigation error model

This section summarises the 15th order INS error model for completeness, which is introduced in Titterton and Weston (2004) in detail. Note that the reference frame is aligned with the north-east-down (NED) geodetic axes, while the body frame is aligned with IMU axes. The submatrices in Equation (10) are presented as from Equations (A1)–(A11):

$$F_{pp} = \begin{bmatrix} \dfrac{\rho_E R_{mm}}{R_m + h} & 0 & \dfrac{\rho_E}{R_m + h} \\ \dfrac{\rho_D}{\cos L} - \dfrac{\rho_N R_{tt}}{(R_t + h)\cos L} & 0 & -\dfrac{\rho_N}{(R_t + h)\cos L} \\ 0 & 0 & 0 \end{bmatrix}, \tag{A1}$$

$$F_{pv} = \begin{bmatrix} \dfrac{1}{R_m + h} & 0 & 0 \\ 0 & \dfrac{1}{(R_t + h)\cos L} & 0 \\ 0 & 0 & -1 \end{bmatrix}, \tag{A2}$$

https://doi.org/10.1017/S0373463322000431 Published online by Cambridge University Press

$$F_{vp} = \begin{bmatrix} \dfrac{\rho_E R_{mm}}{R_m + h} v_D - \left(2\Omega_N + \rho_N \sec^2 L + \dfrac{\rho_D R_{tt}}{R_t + h}\right) v_E & 0 & \dfrac{\rho_E}{R_m + h} v_D - \rho_D \rho_N \\ \left(2\Omega_N + \rho_N \sec^2 L + \dfrac{\rho_D R_{tt}}{R_t + h}\right) v_N + \left(2\Omega_D - \dfrac{\rho_N R_{tt}}{R_t + h}\right) v_D & 0 & \dfrac{\rho_D v_N - \rho_N v_D}{R_t + h} \\ -2\Omega_D v_E + \rho_E^2 R_{mm} + \rho_N^2 R_{tt} + \dfrac{\partial g_0 / \partial L}{(1 + h/R)^2} & 0 & \rho_E^2 + \rho_N^2 - \dfrac{2g_0}{R(1 + h/R)^3} \end{bmatrix}, \quad \text{(A3)}$$

$$F_{vv} = \begin{bmatrix} \dfrac{v_D}{R_m + h} & 2\Omega_D + 2\rho_D & -\rho_E \\ -2\Omega_D - \rho_D & \dfrac{v_N \tan L + v_D}{R_t + h} & 2\Omega_N + \rho_N \\ 2\rho_E & -2\Omega_N - 2\rho_N & 0 \end{bmatrix}, \quad \text{(A4)}$$

$$F_{v\varphi} = \begin{bmatrix} 0 & -f_D & f_E \\ f_D & 0 & -f_N \\ -f_E & f_N & 0 \end{bmatrix}, \quad \text{(A5)}$$

$$F_{vb} = C_b^n, \quad \text{(A6)}$$

$$F_{\varphi p} = \begin{bmatrix} \Omega_D - \dfrac{\rho_N R_{tt}}{R_t + h} & 0 & -\dfrac{\rho_N}{R_t + h} \\ -\dfrac{\rho_E R_{mm}}{R_m + h} & 0 & -\dfrac{\rho_E}{R_m + h} \\ -\Omega_N - \rho_N \sec^2 L + \dfrac{\rho_D R_{tt}}{R_t + h} & 0 & \dfrac{\rho_D}{R_t + h} \end{bmatrix}, \quad \text{(A7)}$$

$$F_{\varphi v} = \begin{bmatrix} 0 & \dfrac{1}{R_t + h} & 0 \\ -\dfrac{1}{R_m + h} & 0 & 0 \\ 0 & -\dfrac{\tan L}{R_t + h} & 0 \end{bmatrix}, \quad \text{(A8)}$$

$$F_{\varphi\varphi} = \begin{bmatrix} 0 & \Omega_D + \rho_D & -\rho_E \\ -\Omega_D - \rho_D & 0 & \Omega_N + \rho_N \\ \rho_E & -\Omega_N - \rho_N & 0 \end{bmatrix}, \quad \text{(A9)}$$

$$F_{\varphi b} = -C_b^n, \quad \text{(A10)}$$

$$F_{cc} = \begin{bmatrix} -1/T_c & 0 & 0 \\ 0 & -1/T_c & 0 \\ 0 & 0 & -1/T_c \end{bmatrix}, \quad \text{(A11)}$$

where $R_m = R_0(1 - e^2)/(1 - e^2 \sin^2 L)^{3/2}$, $R_t = R_0/(1 - e^2 \sin^2 L)^{1/2}$, $R_{mm} = (\partial R_m / \partial L) = 3(R_0(1 - e^2)(e^2 \sin L \cos L)/(1 - e^2 \sin^2 L)^{5/2})$, $R_{tt} = (\partial R_t / \partial L) = (R_0 e^2 \sin L \cos L / (1 - e^2 \sin^2 L)^{3/2})$, $\Omega_N = \Omega_{ie} \cos L$, $\Omega_D = -\Omega_{ie} \sin L$, $\rho_N = v_E / R_t + h$, $\rho_E = -(v_N / (R_m + h))$, $\rho_D = -(v_E \tan L / (R_t + h))$.

https://doi.org/10.1017/S0373463322000431 Published online by Cambridge University Press

B. Appendix B: Sea current model and navigation performance

In this section, a simplified one-dimensional sea current relative navigation problem is dealt with to analyse the effect of the standard deviation of sea currents of the first-order Markov model. That is, instead of Equation (6), we define a state vector as Equation (B1):

$$x = \begin{bmatrix} v & v_c \end{bmatrix}^T \in \mathbb{R}^2. \tag{B1}$$

Hence, the measurement model in Equation (11) is simplified to Equation (B2):

$$\rho = v - v_c + \eta. \tag{B2}$$

By substituting this into the Kalman filtering process of Equation (23), the variance for the velocity of the vehicle can be obtained as Equation (B3):

$$P_{11}^{+} = P_{11}^{-} - \frac{(P_{11}^{-} - P_{12}^{-})^2}{P_{11}^{-} - 2P_{12}^{-} + P_{22}^{-} + R} \tag{B3}$$

where P_{ij} indicates the $(i, \ j)$-th element of P. Although P_{11}^{-} is independent of the sea current model by Equation (10), as the standard deviation of sea current increases, P_{22}^{-} and P_{11}^{+} increase consequently. In other words, it implies that even if the filter was optimally designed, the guaranteed performance improvement due to the aid of an EM-log or a DVL inevitably decreases as the standard deviation of the sea current increases.

Cite this article: Cha J, Hwang JH, Park CG (2022). Sea current relative navigation using interacting multiple model filter with adaptive fading technique. *The Journal of Navigation* **75**: 5, 1190–1205. https://doi.org/10.1017/S0373463322000431

https://doi.org/10.1017/S0373463322000431 Published online by Cambridge University Press